



Full Length Article



Comparison of thermophysical properties and combustion characteristics of various biodiesels in a non-MILD ultra-low emission swirl burner

Gyöngyvér Tóthpálné Hidegh^a, Dávid Csemány^{a,*}, Osama DarAli^a, Syed Ali Hamza Rizvi^a, Jo-Han Ng^b, Cheng Tung Chong^c, Viktor Józsa^a

^a Budapest University of Technology and Economics, Faculty of Mechanical Engineering, Department of Energy Engineering, 1111 Budapest, Műegyetem rkp. 3., Hungary

^b Faculty of Engineering and Physical Sciences, University of Southampton Malaysia (UoSM), 79100 Iskandar Puteri, Johor, Malaysia

^c China-UK Low Carbon College, Shanghai Jiao Tong University, Lingang, Shanghai 201306, China

ARTICLE INFO

Keywords:

Evaporation
Volatility
Distillation
Distributed combustion
Biodiesel
Mixture temperature-controlled

ABSTRACT

All global decarbonization strategies increase the importance of biodiesels in the future. Presently, three representative biodiesels: coconut, oil palm, and waste cooking oil, were studied. The coconut methyl ester is the most volatile, while palm methyl ester is among the least volatile biodiesels. The waste cooking oil-based biodiesel has a highlighted presence in the circular economy. Firstly, the thermophysical properties of the three neat biodiesels and blends with commercial diesel fuel are presented. Density, surface tension, and kinematic viscosity affect atomization, and the distillation curve characterizes fuel evaporation, while the flash point is critical for mixture ignition. The fuels behaved similarly up to 25 V/V% biodiesel-diesel mixture. Secondly, all fuels are tested in a Mixture Temperature-Controlled burner, featuring distributed combustion without any low-oxygen technique. The flame shape was highly affected by fuel volatility and governed pollutant emissions. NO emission was evaluated due to practically complete combustion in all cases, concluding that distributed combustion may lead to nearly a magnitude reduction of this pollutant. The maximum value was below 14 mg/Nm³, fulfilling the current European gas turbine standard with an 80% margin. Our goal is to introduce the Mixture Temperature-Controlled combustion concept in boilers and gas turbines.

1. Introduction

Our recent efforts toward a carbon-neutral future are aggressive, but it is uncertain when this goal can be achieved. A deep decarbonization plan aims for 2050 [1], while the change may require the entire 21st century [2]. As the essential solutions and infrastructure are globally emerging, careful advancement of the current technologies is critical to start decreasing their carbon footprint as soon as possible while maintaining the service and covering our ever-increasing hunger for energy [3]. Moreover, hydrocarbon combustion plants remain essential to keep the electricity prices at a reasonable level, even at zero allowed CO₂ emission [4]. Nitrogen oxides mean 4% of the total emissions [5], with a side note that 3/4 of the N₂O emission is related to agriculture, while transportation and industrial uses are responsible for the rest [6]. NO, and NO₂, referred to together as NO_x, have a global warming potential of 30–33 over 20 years, dropping to 7–10 over 100 years, compared to CO₂. However, NO_x is excluded from the list of greenhouse gases today [5]. Nevertheless, its adverse effect on human health, the ozone layer

destruction at high altitudes, and soil and water acidification cannot be overlooked. Consequently, the cleanest possible operation besides the extensive use of alternative fuels is still desired, calling for advanced combustion concepts.

The desire for perfect and complete combustion, i.e., no excess fuel and oxidizer remains, and the conversion takes place with 100% efficiency, was known from the beginning of combustion research. However, practical problems caused deviations from the ideal case. Non-premixed burners feature high emissions, and they are easy and safe to operate. The state-of-the-art industrial burners feature highly premixed, swirling flames for low emissions [7]. To overcome the problem of locally high temperatures and exponentially increasing NO_x emission [8], the Moderate or Intense, Low-oxygen Dilution, MILD, combustion concept was introduced [9]. Even though it is a highly potential concept for future use [10], its use in gas turbine technology requires solving difficult technical problems [11]. Our research group has recently introduced the Mixture Temperature-Controlled, MTC, combustion concept [12], which offers similar flame characteristics to MILD combustion for liquid fuels [13] and provides ultra-low emissions. However,

* Corresponding author.

E-mail address: csemany@energia.bme.hu (D. Csemány).

<https://doi.org/10.1016/j.fuel.2022.126583>

Received 21 August 2022; Received in revised form 7 October 2022; Accepted 29 October 2022

0016-2361/© 2022 The Author(s). Published by Elsevier Ltd. This is an open access article under the CC BY license (<http://creativecommons.org/licenses/by/4.0/>).

Nomenclature		WCO	Waste cooking oil
Latin letters Names, Unit (if relevant)		We	Weber number, 1
ALR	Air-to-liquid mass flow ratio, 1	<i>Greek symbols</i>	
C	Correlation coefficient, 1	ϕ	Equivalence ratio, 1
CME	Coconut oil methyl ester	μ	Mean value, (varies)
D	Diesel fuel	ν	Kinematic viscosity, m ² /s
<i>d</i>	Characteristic diameter, m	ρ	Density, kg/m ³
DC	Distillation curve	σ	Surface tension, N/m
FAME	Fatty acid methyl ester	<i>Subscripts</i>	
MTC	Mixture Temperature-Controlled	<i>a</i>	Atomizing air
Oh	Ohnesorge number, 1	<i>ca</i>	Combustion air
<i>p</i>	Pressure, bar	<i>FP</i>	Flash point
PME	Palm oil methyl ester	<i>g</i>	Gauge
Re	Reynolds number, 1	<i>IBP</i>	Initial boiling point
<i>SMD</i>	Sauter mean diameter, m	<i>L</i>	Liquid-phase
std	Standard deviation, (varies)	<i>m</i>	Mixture
<i>T</i>	Temperature, °C	<i>mt</i>	Mixing tube
<i>V</i>	Volume fraction, %		
<i>w</i>	Mean velocity, m/s		

there is no need for oxygen dilution, and the inlet mixture temperature is below the autoignition temperature. The MTC burner offers distributed combustion, i.e., the local equivalence ratio is approaching to the global equivalence ratio in the entire combustion chamber. Therefore, this paper investigates the effect of various biodiesel fuels on their combustion characteristics.

In our current vision of a sustainable economy, alternative fuels always come up due to the heavy industry and transportation, which are especially hard to decarbonize [14]. The most mature candidate is biodiesel [15–17], which is expected to remain the principal alternative fuel in the upcoming decade as the current diesel engines are highly compatible with them [18]. Keeping in mind that fuel production should not compete with food (first-generation biofuels) [19], biofuel production focuses on increasing the share of alternative sources [20,21]. Examples are agricultural wastes and industrial biowastes (second-generation biofuels), as stipulated in the Renewable Energy Directive (RED) II [22]. The expectations are high for algae biofuels (third-generation biofuels) since the oceans are not cultivated yet [23]. Since power-to-liquid fuels are practically absent [24], it is improbable that such fuels will soon have general and global market penetration with current technologies. Nevertheless, the ReFuelEU initiative [25] requests 0.7 V/V% of such fuels from 2030 in aviation kerosene. The principal products of both edible and non-edible oil seeds and algae are oils with varying triglyceride compositions. Biodiesel production from them is a straightforward step since the conversion needs only 1% of the heating value on an energy basis to end up with an easy-to-handle fuel [26]. Moreover, this value can be further suppressed if waste heat is used. Therefore, the results of the presented biodiesels in Section 2 can be indirectly used for fuels with a similar chemical composition of highly different geographical and biological origins.

If the reaction temperature exceeds 1000 K, fuel composition shows a marginal theoretical effect on the process of hydrocarbon combustion if there is sufficient residence time [27,28]. If liquid fuels are utilized, they have to be atomized and then evaporated before reaching the flame front. However, the difference in these processes may lead to variation in the mixture quality, ultimately determining the flame characteristics and emissions [29]. For this reason, the relevant thermophysical properties of all the investigated fuels are measured.

Palm oil methyl ester, PME, is produced in the largest quantity around the globe, and 85% of it originates from Indonesia and Malaysia [30]. For this reason, this fuel type was the first to be investigated. The fatty acid composition of most biodiesels peaks at C₁₈ fatty acids, while

PME is an exception with C₁₆ and coconut oil methyl ester, CME, with C₁₂ [31]. Finally, the mixture of rapeseed and sunflower oil-originated waste cooking oil-derived methyl ester, abbreviated as WCO, was investigated in the framework of this study. Their composition and properties are discussed in Subsections 2.2, 3.1, and 3.2. Since biofuels cannot cover our liquid fuel needs, various mixtures with commercial diesel fuel, D, in 25 V/V% steps were investigated. It has to be emphasized that this paper is principally not about increasing the utilization of first-generation biofuels but about testing various samples and their effect on combustion. CME is an outlier, and all other practical biodiesels are closer to PME in chemical composition. Therefore, their fatty acid methyl ester, FAME, content is concentrated in the C₁₆-C₁₈ carbon chain length regime, including saturated and unsaturated variants of these methyl esters.

This paper focuses on two fields. Firstly, the thermophysical properties of three different biodiesel fuels were investigated, essential to estimate atomization characteristics, evaporation, and mixing with combustion air in numerical software. Furthermore, liquid fuel data is often scarce at elevated temperatures or for mixtures with D. Presently, density, viscosity, surface tension, distillation curve, and flash point of PME, CME, and WCO and their blends with D were measured. Secondly, the combustion characteristics of all the mentioned neat and blended fuels are evaluated in an MTC burner, allowing ultra-low emissions if the conditions of distributed combustion are met, even with fuels with low volatility. Distributed combustion is frequently connected to MILD combustion in the literature, while these are different terms. The used burner is the first to achieve distributed combustion without needing low-oxygen conditions with either internal or external recirculation. Moreover, using liquid fuels with moderate volatility demonstrates its superiority and maturity for industrial use in boilers, gas turbines, and other combustion systems.

2. Materials and methods

This section is divided into three parts. Subsection 2.1 details the combustion test rig with the corresponding diagnostic apparatus and the operating parameters. Subsection 2.2 summarizes the measurement methods of fuel properties affecting spray formation, droplet evaporation, and ignition, the investigated biodiesel types, and their FAME compositions. Finally, droplet size characteristics of the spray are discussed in Subsection 2.3.

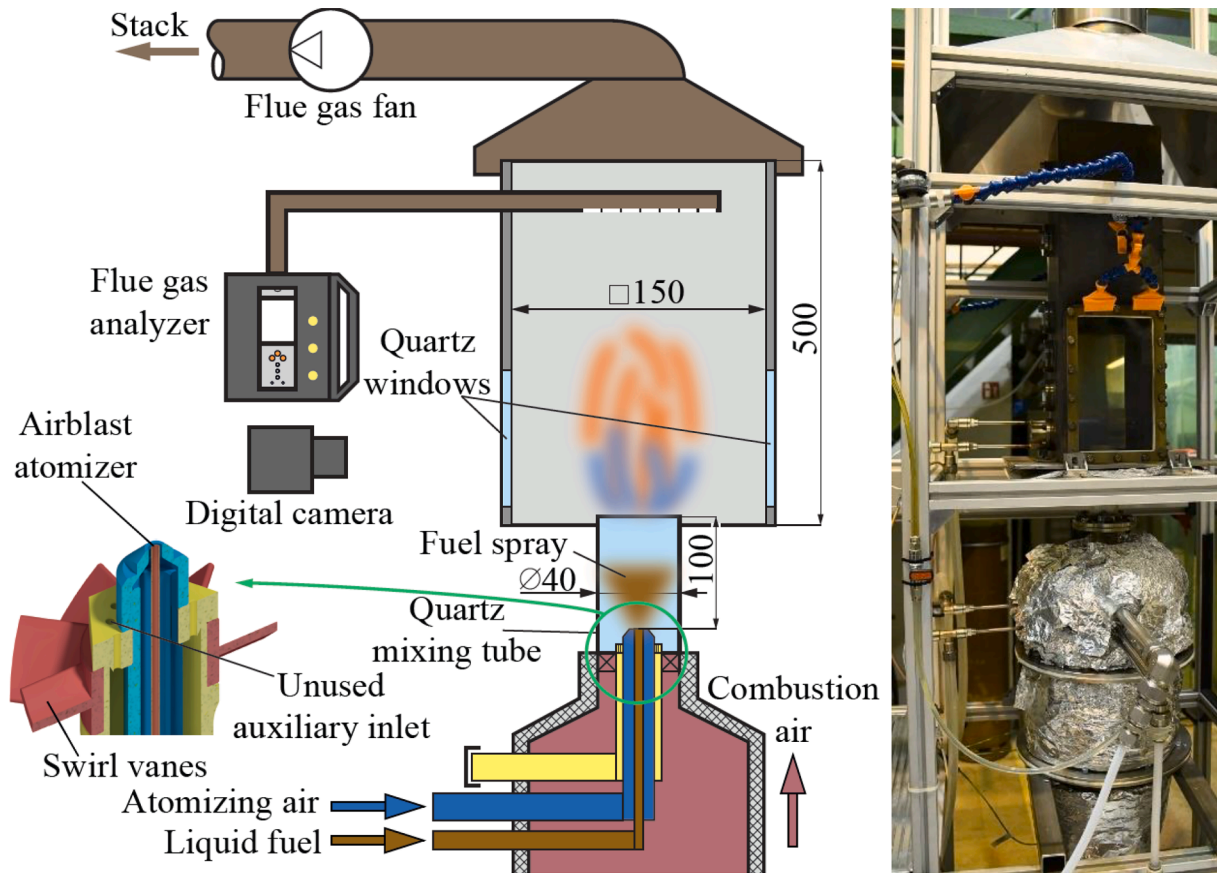


Fig. 1. Schematic diagram of the test rig (left) [32]. All units are in mm. A photo of the system (right).

Table 1
Test conditions.

Parameter	Value/range
Thermal power [kW]	13.3
Fuel types	D, CME, PME, and WCO
Blends	B25, B50, and B75
ϕ [1]	0.8
T_{ca} [°C]	150–350
Re [1]	6396–8316
p_g [bar]	0.3–0.9
SMD [μm]	19.4–38.1
ALR [1]	1.26–2.67

2.1. Experimental setup

The test rig is shown in Fig. 1 and detailed in [32], including measurement uncertainties. The flow is fully turbulent, indicated by the Reynolds number, calculated as:

$$Re = \frac{w_m \cdot d_{mt}}{\nu_m}, \quad (1)$$

where w_m is the mixture mean velocity, d_{mt} is the mixing tube inner diameter, and ν_m is the mixture kinematic viscosity. The Re range and the other characteristic parameters of the combustion tests are included in Table 1.

The combustion air was preheated by an electric heater to $T_{ca} = 150\text{--}350$ °C; this temperature was measured upstream of the swirl vanes and before the converging part of the flow homogenizer, using a standard K-type thermocouple with a standard uncertainty of $\max(2.2, T \times 0.0075)$ in °C). The uncertainty matched this specification after calibration. Since the plenum was insulated and had no

visible access to the flame, thermal radiation causes no bias after warming up before the measurements. The gauge pressure of the atomizing air, p_g , varied in the range of 0.3–0.9 bar with 0.3 kPa measurement uncertainty at a 95% significance level. The equivalence ratio, ϕ , was kept constant at 0.8, and the thermal power was uniformly 13.3 kW. The most widely used characteristic dimension in liquid fuel atomization is the Sauter mean diameter, SMD , which varied from 19.4 to 38.1 μm . The air-to-liquid mass flow ratio, ALR , of the atomizer varied in the range of 1.26 to 2.67. Therefore, the combustion air flow rate had to be adjusted to keep ϕ constant. The details of SMD estimation are included in Subsection 2.3, and the results can be found in Subsection 3.1. Besides the neat fuel samples of D, CME, PME, and WCO, their blends with D in 25, 50, and 75 V/V% were also investigated, abbreviated as B25, B50, and B75, referring to the biodiesel volume fraction in the mixture. B100 is used for neat biodiesels. Since multiple biodiesels were tested, the abbreviated name of the neat fuel is added to the concentration as a prefix. Note that phase separation was not observed in any case; all blends were perfectly miscible.

The investigated WCO-B100 was produced from 40 V/V% of waste cooking oil containing sunflower and rapeseed cooking oil and 60 V/V% crude rapeseed oil to fulfill the corresponding standards. Consistent quality was essential for the company that supplies all the Hungarian petrol stations with the mandatory biodiesel share, according to the EN 590:2017 standard. This is B7 or a similar value in numerous countries around the globe.

An Omega FPD3202 positive displacement flow meter measured the fuel flow rate with < 3% uncertainty at a 95% significance level. The ALR range meant 22.8–45 slpm flow rate with an Omega FMA1842 mass flow meter, measured with 1 slpm uncertainty with factory calibration.

A Testo 350 flue gas analyzer was used for pollutant emission

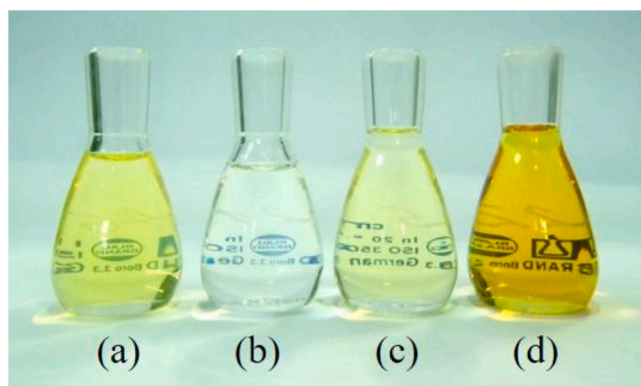


Fig. 2. Neat samples: (a) D, (b) CME-B100, (c) PME-B100, and (d) WCO-B100.

measurement, having 0.2 V/V% uncertainty for O_2 , which was the basis of calculating ϕ . Further relevant uncertainties were 3 ppm for CO and 2 ppm for NO after calibration with special gases by Linde. Since the CO emission was around 10 ppm or lower and showed random behavior, this pollutant was not presented. These values are very low compared to the 100 ppm limit set by the Hungarian 53/2017 directive, which will not be further reduced in the upcoming regulation from 2025. The closely equivalent European EC 2015/2193 [33] directive does not contain any restrictions on CO emissions. The unburnt hydrocarbon emission was checked in a few characteristic points with 2–3 ppm values by a calibrated Horiba MEXA 8120 automotive flue gas analyzer system, which was its uncertainty. Based on the very low CO and unburnt hydrocarbon concentrations in the flue gas, combustion can be considered practically complete in all cases. Consequently, only NO emission is discussed further, which significantly varied with measurement setup and flame shape.

Table 2

Experimental setups for kinematic viscosity, density, surface tension, flash point, distillation curve, and initial boiling point.

	Apparatus	Method	T control	Uncertainty	Standard deviation
ν_L	Cannon-Fenske viscometer	ASTM D445-06, ASTM D446-07	Silicone oil bath, thermostat, pump	0.09 mm ² /s, 2 °C	0.008 mm ² /s
ρ_L	Gay-Lussac pycnometer, Sartorius laboratory balance	ISO 3507:1999, ISO4787:2010	Silicone oil bath, thermostat, pump	1.6 kg/m ³ , 2 °C	0.3 kg/m ³
σ	Krüss DSA30 drop shape analyzer, Stingray F046B IRF digital camera	Pendant droplet	thermostat, pump	2 °C	0.06 mN/m
T_{FP}	Cleveland open-cup tester, Voltcraft K102 digital thermometer	DIN 51 and 376, IP 36, ASTM D92	–	2 °C	0.8 °C
DC, T_{IBP}	atmospheric distillation apparatus, heating mantle, K-type thermocouple	ASTM D86	–	0.5% in T [°C], 5 ml in volume	3 °C

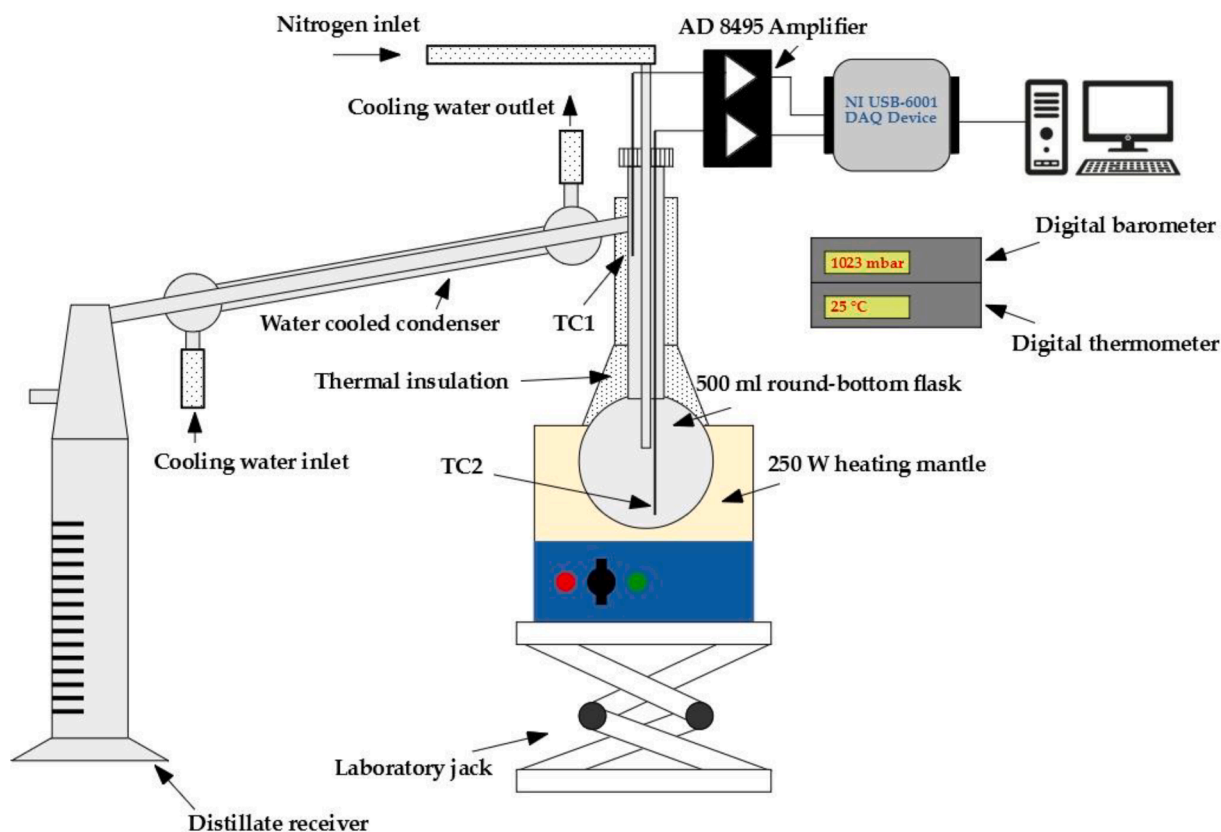
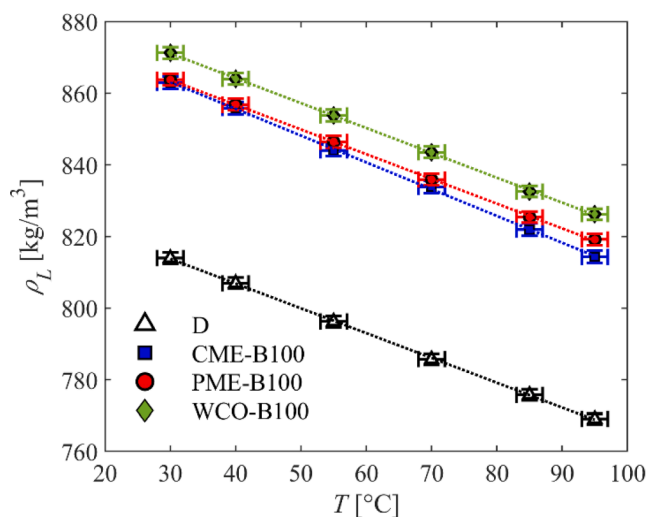
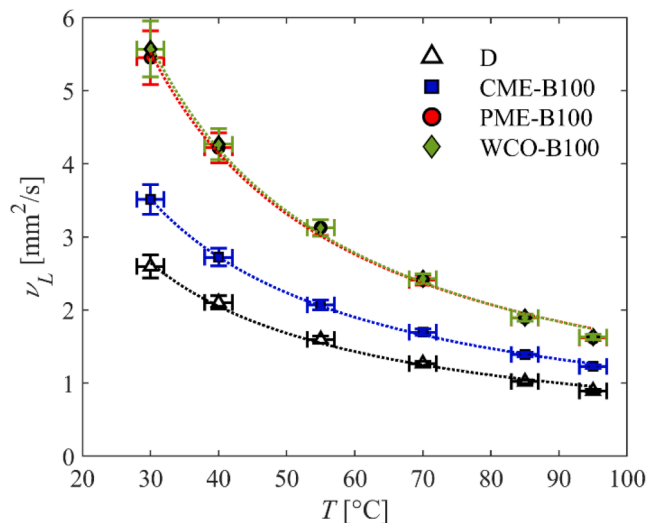


Fig. 3. The atmospheric distillation apparatus with inert gas injection.

Table 3

Fatty acid methyl ester composition of the investigated biodiesel samples in mass percentage.

Fatty acid component	CME-B100	PME-B100	WCO-B100
C8:0	6.78	0	0
C10:0	5.61	0	0
C12:0	51	0	0
C14:0	18.51	0.93	0.31
C16:0	9.26	39.85	12.77
C16:1	0	0	0.31
C18:0	1.66	3.55	3.50
C18:1	6.06	43.14	46.96
C18:2	1.12	12.53	31.72
C18:3	0	0	2.57
C20:0	0	0	0.41
C20:1	0	0	0.62
C22:0	0	0	0.51
C24:0	0	0	0.21
C24:1	0	0	0.11

**Fig. 4.** Density of neat samples.**Fig. 5.** Kinematic viscosity of neat samples.

2.2. Measurement of fuel properties

Fig. 2 shows the neat fuel samples. Table 2 summarizes the measurement apparatus, method, temperature control, uncertainty, and standard deviation of kinematic viscosity, ν_L , density, ρ_L , surface tension, σ , flash point, T_{FP} , distillation curve, DC, and initial boiling point, T_{IBP} , measurements. Further information on the experimental equipment, calibration, error estimation, repeatability of the measurements, and preliminary tests to verify the setups are available in [34].

The volatility characteristics of the samples were evaluated by DC, and T_{IBP} measurements with a modified ASTM D86 atmospheric distillation apparatus, shown in Fig. 3. Vapor and liquid temperatures were measured with calibrated K-type thermocouples, TC1 and TC2, respectively. The setup is identical to the one used in [34]. The whole apparatus was flushed with nitrogen before heating was applied to remove oxygen and prevent gum formation and the thermal decomposition of methyl ester molecules. The nitrogen valve was then closed. Therefore, all the measurements were performed in a nitrogen atmosphere, and no fuming was observed, which indicates thermal decomposition. T_{IBP} is the liquid temperature at the very beginning of the boiling process. It was identified according to the considerations detailed in [34] from the sudden increase of vapor temperature monitored by TC1. Note that the temperatures related to distillation curves and T_{IBP} discussed later are all liquid temperatures measured with TC2 to approximate the true thermodynamic conditions and vapor–liquid equilibrium.

Table 3 shows the FAME composition of the investigated biodiesel samples, measured by the gas chromatography-mass spectrometry method. The values refer to the mass percentage of the methyl esters of the fatty acids listed in the first column, e.g., C8:0 is caprylic acid, and its methyl ester is methyl octanoate (methyl caprylate, $C_9H_{18}O_2$). The yields in the gas chromatography analysis were 96.9%, 97.9%, and 97.1% for CME-B100, PME-B100, and WCO-B100, respectively, due to the FAME components with extremely low volatility. No notable methanol content from the production process and other impurities were identified. Therefore, the values in Table 3 are normalized to 100%. Generally, CME-B100 contains shorter-chain FAMES. Methyl dodecanoate (methyl laurate) is the most dominant with 51%, and the methyl tetradecanoate (methyl myristate) content is also significant with 18.51%. PME-B100 and WCO-B100 share highly similar FAME compositions. Methyl oleate content is the highest in both samples, with 43.14% and 46.96%. However, the second most significant component is methyl hexadecanoate (methyl palmitate) in PME-B100 and methyl linoleate in WCO-B100 with 39.85% and 31.72%, respectively. It results in a slightly higher average molecular mass of WCO-B100.

2.3. Droplet size estimation

The SMD of airblast atomizers is often estimated based on the following semi-empirical formula [35]:

$$\frac{SMD}{d_L} = (C_1 \cdot We_a^{-0.5} + C_2 \cdot Oh) \cdot \left(1 + \frac{1}{ALR}\right), \quad (2)$$

where d_L is the initial diameter of the liquid jet, We_a is the Weber number with the subscript a , which notes atomizing air, Oh denotes the Ohnesorge number, and C_1 and C_2 coefficients are obtained from [36]. We_a and Oh were calculated as:

$$We_a = \frac{\rho_a \cdot d_L \cdot w_a^2}{\sigma} \quad (3)$$

$$Oh = \nu_L \sqrt{\frac{\rho_L}{\sigma \cdot d_L}} \quad (4)$$

where w_a is the mean velocity of the atomizing air, ρ_a represents the density of atomizing air, ρ_L is the liquid jet density, and σ denotes the surface tension.

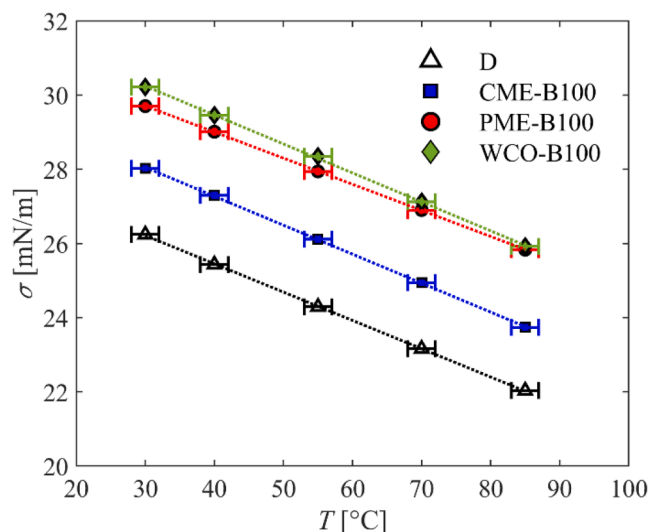


Fig. 6. Surface tension of neat samples.

3. Results and discussion

This section is divided into three parts. Subsection 3.1 presents the fuel properties affecting spray formation and the estimated *SMD* values for all tested fuels. Volatility characteristics influencing droplet evaporation are shown in Subsection 3.2. All the experimental data on fuel properties with the corresponding uncertainty values are available in the following online repository [37]. Subsection 3.3 summarizes the results of the combustion tests, including flame shapes and exhaust gas emissions. Moreover, the observed flame shape regions are evaluated in light of the differences in fuel properties. Finally, a correlation analysis between the NO emission of various fuels is presented.

3.1. Density, viscosity, surface tension, and the estimated Sauter mean diameter

SMD estimation requires thermophysical and transport properties, which are presented first. Figs. 4–6 show ρ_L , ν_L , and σ of the neat samples. Dotted lines represent fitted model equations discussed in Appendix A with all parameter values. The trends for ρ_L are relatively similar for the different biodiesel samples in the investigated temperature range. The difference is within 2% at each temperature, shown in Fig. 4. However, D has a lower density than biodiesels. The ν_L of PME-B100 and WCO-B100 are practically identical, as shown in Fig. 5, due to the highly similar FAME composition. As for CME-B100, ν_L is 25–35% lower than that of the other two biodiesels and 25% higher than that of D, resulting from the shorter-chain methyl ester components. In general, higher molecular mass components significantly increase ν_L , compared to D, leading to larger average droplet sizes in atomization [35]. Fig. 6 shows σ . PME-B100 and WCO-B100 differ only by 2% from each other, while σ of CME-B100 and D is 8% and 14% lower in the investigated temperature range. The measured values of ρ_L , ν_L , and σ of the investigated blends are presented in Appendix B.

Fig. 7 presents the calculated *SMD* values of the investigated blends at 30 °C liquid temperature, according to Eq. (2), since no fuel pre-heating was applied. PME and WCO blends show identical characteristics due to their very similar FAME compositions. CME blends possess lower values, resulting from the markedly lower ν_L . However, the different biodiesels show matching trends up to B25 despite the different FAME compositions of CME and the other two B100 samples, which fosters fuel flexibility concerning the feedstock.

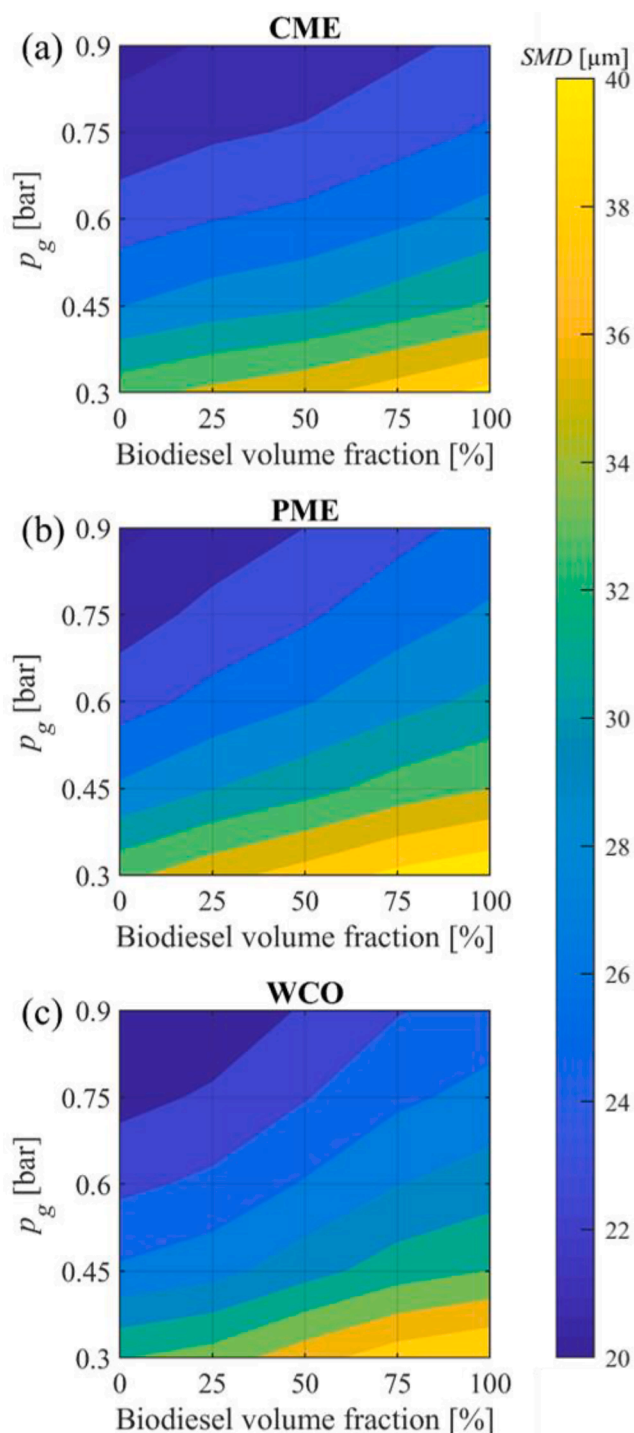


Fig. 7. Calculated *SMD* values of (a) CME, (b) PME, and (c) WCO blends at 30 °C liquid temperature.

3.2. Fuel volatility

Figs. 8–10 show the distillation curves of CME, PME, and WCO blends. The volatility characteristics of PME-B100 and WCO-B100 are almost identical and flat, as shown in Figs. 9 and 10 due to the practically similar FAME compositions. These two samples were the least volatile among the investigated ones. Their boiling temperature ranges are relatively high and narrow compared to that of CME-B100 and D, which are more volatile than the former ones. CME-B100 is similar to D due to the shorter-chain methyl ester components, as shown in Fig. 8.

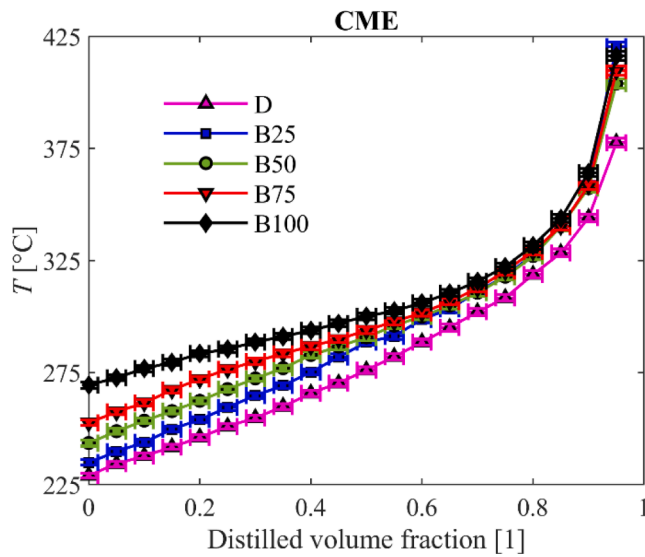


Fig. 8. Distillation curves of CME blends.

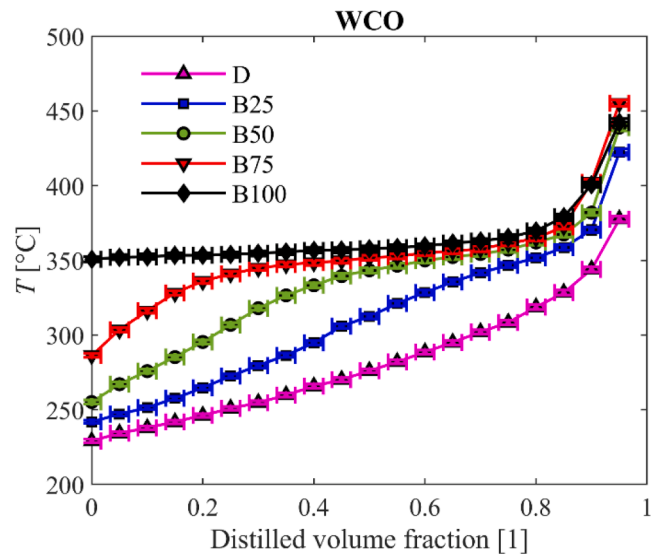


Fig. 10. Distillation curves of WCO blends.

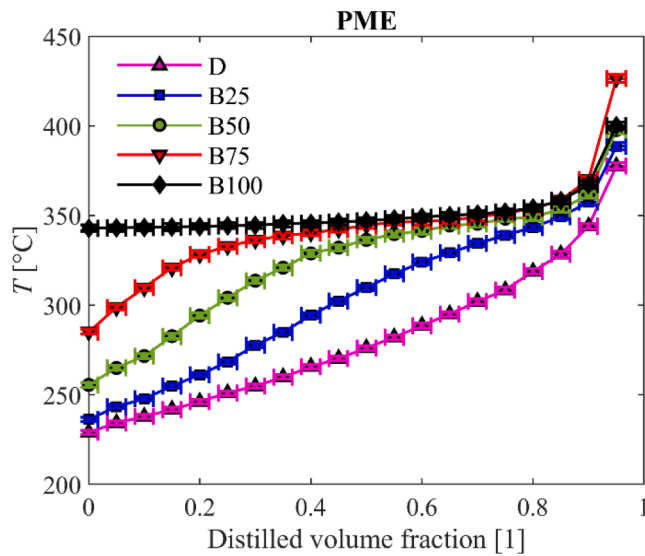


Fig. 9. Distillation curves of PME blends.

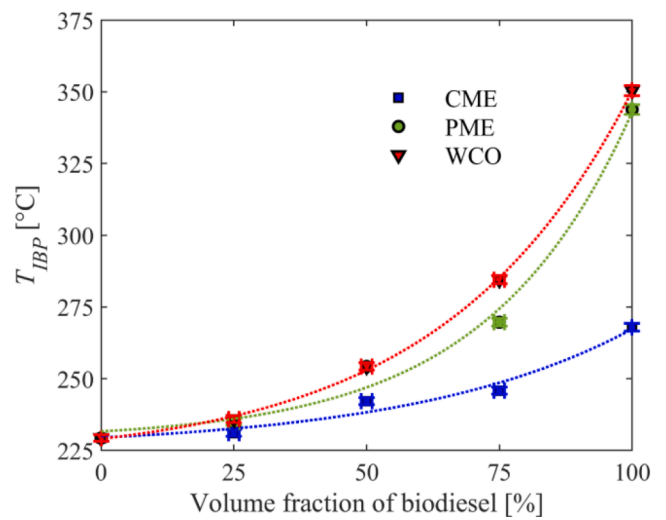


Fig. 11. Initial boiling point of all tested fuels.

The FAME composition of CME-B100 is highly similar to the CME sample investigated by Bachler et al. [38]. Volatility affects droplet evaporation in spray combustion; thus, a higher combustion air temperature might be necessary in the case of PME-B100 and WCO-B100 to achieve a similar flame to D [29].

Both PME-B100 and WCO-B100 are much less volatile than D; hence, blending has a more significant impact on the distillation curves and is more spectacular than in the case of CME. The blends of PME-B100 and WCO-B100 and D practically match. For all the investigated blends, as the volume fraction of biodiesel increases, the early-stage regime of the distillation curves shows a nonlinear increase from D to B100. Note that PME-B75 and WCO-B75 required the highest temperature for the maximum distilled fraction. The reason for that is a possible dry-out of the TC2 thermocouple due to the small amount of residual liquid at the end. This results in higher measurement bias due to the thermal radiation of the hot heating mantle. Otherwise, all B75 trends remain below the respective B100 trends.

The exponential trend of T_{IBP} with the increase of biodiesel volume fraction is presented in Fig. 11. Dotted lines represent curve fitting applicable for further calculations. The coefficients are detailed in

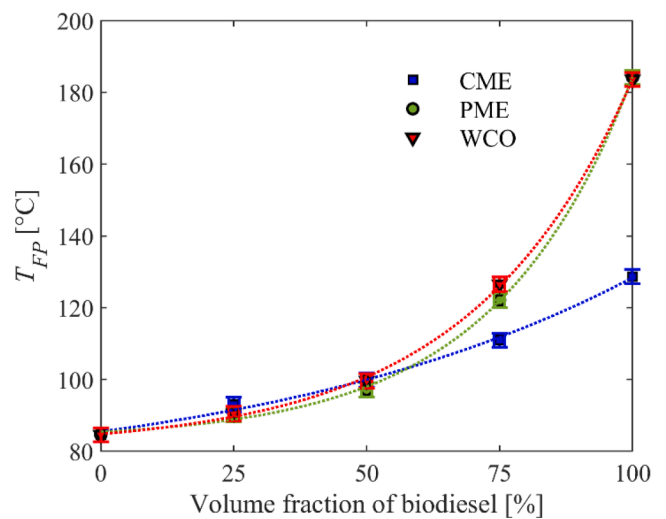


Fig. 12. Flash point of all tested fuels.

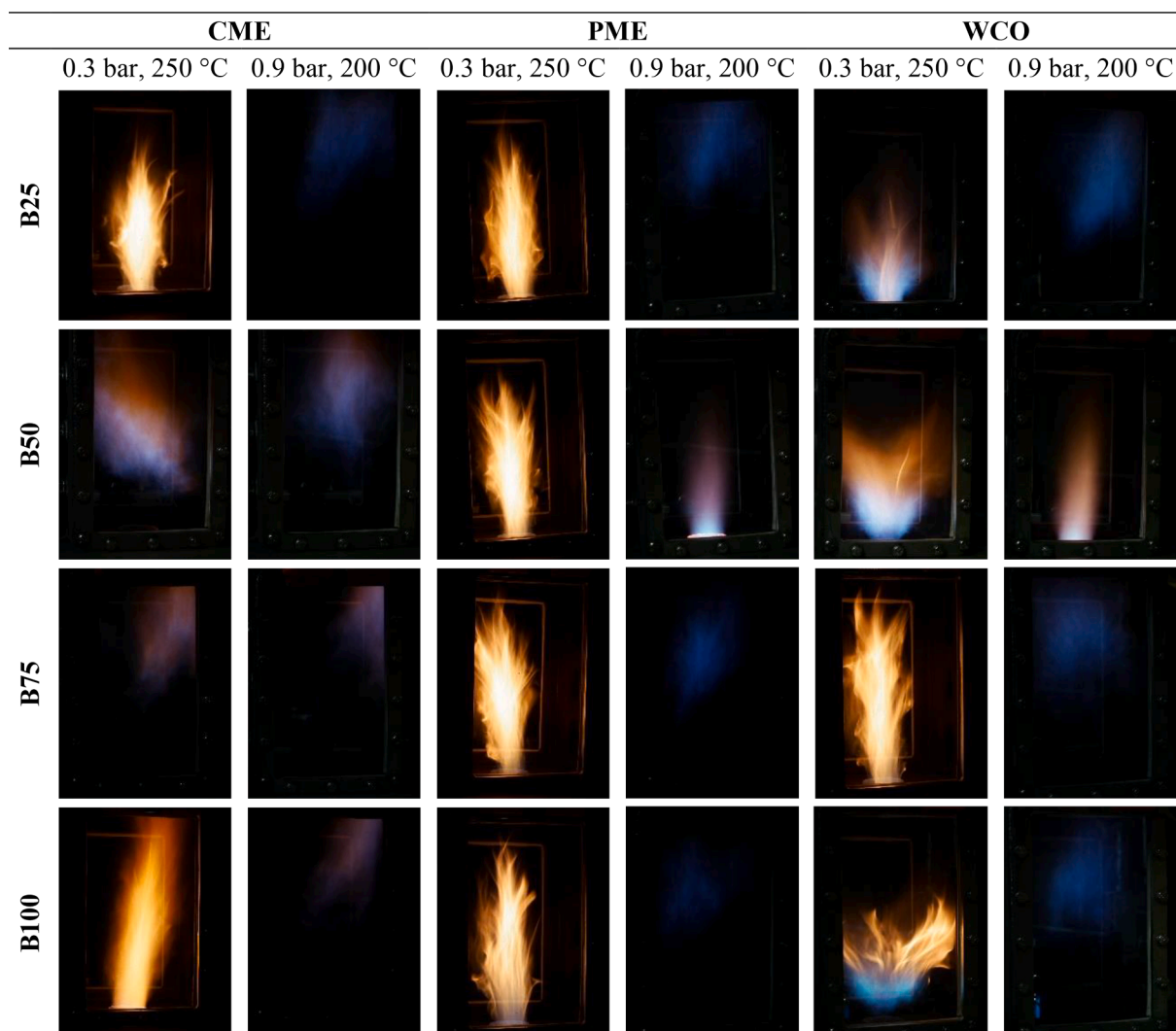


Fig. 13. Selected flame images. The visible size of the front quartz window is 112×193 mm.

Appendix A. PME and WCO blends are similar, while CME blends are more volatile, resulting in lower T_{IBP} values. However, the difference in T_{IBP} between the investigated biodiesels is practically within the measurement uncertainty up to B25. Therefore, the effect of biodiesel composition is not significant in this regime, biodiesels from different feedstocks blended with the same diesel fuel show similar volatility characteristics. This may allow manufacturers to diversify the feedstock in countries where biodiesel is blended with standard diesel oil within this regime. FAME composition has no significant influence, promoting the utilization of non-first-generation biodiesels, such as WCO.

Fig. 12 shows T_{FP} of the investigated blends as a function of biodiesel volume fraction. Similar to T_{IBP} , an exponential behavior can be observed here. The curve fitting parameters are detailed in Appendix A. Values of PME and WCO blends match again, while CME blends have lower T_{FP} . The difference is negligible up to B50 for all biodiesel blends, meaning that the FAME composition has no considerable influence up to this volume fraction. Since flash point characterizes volatility and flammability, biodiesel blends in this regime meet the same safety regulations regardless of the feedstock and FAME composition.

3.3. Visual flame characteristics and NO_x emission

Three distinct flame shapes were observed during the combustion tests of CME, PME, and WCO: straight, V-shaped, and distributed. However, stable combustion lasting for at least several minutes occurred

only in the case of straight and distributed flames – a few enduring tests for more than half an hour of operation confirmed this finding. Therefore, the MTC burner offers excellent flame stability for distributed flames, even under highly lean conditions. In the measurement setups where the flame shape was altered, the transition frequency was in the range of 1 Hz between two flame shapes, which is best avoided in industrial applications. Fig. 13 presents selected flame images recorded during the tests. At low p_g , droplet combustion is visible via the flares since their residence time in the mixing tube is insufficient. The soot completely burns out since all flames are lean and there is sufficient residence time in the combustion chamber. After a hundred hours of testing, no soot marks were found on the chamber walls. However, the local high-temperature zones lead to high – up to $90 \text{ mg}/\text{Nm}^3$ at 15% flue gas oxygen content – NO_x formation, typical in luminous, yellow, straight flames.

At higher p_g , smaller droplets are formed, which can completely evaporate in the mixing tube, and a more homogenous fuel–air mixture enters the combustion chamber. The flames are more compact, and the flame color shifts towards purple and then blue. When neat WCO, B50, and B25 were combusted at $p_g = 0.3$ bar, and $T_{ca} = 250$ °C, V-shaped and straight flames were altered. The blue cone of the V-shaped flame can be intermittently seen, as well as the yellow flares of the straight flame.

At $p_g = 0.9$ bar, distributed combustion was observed. These flames feature low luminosity and blue color; the presented images are the luminous ones among a couple of others recorded at each setup. The

D T_{ca} [°C]	p_g [bar]				
	0.3	0.45	0.6	0.75	0.9
350	s-d	s-d	s-d	s-d	s-d
300	s-d	s-d	s-d	s-d	s-d
250	s-d	s-d	s-d	d	d
200	s	s-d	d	d	d
150	s	s	d	d	d

Fig. 14. Observed flame shapes at all diesel measurement points. Abbreviations refer to the stable flame shapes: s – straight (yellow), d – distributed (blue). The straight and distributed (s-d) transitory operation is green [32]. (For interpretation of the references to color in this figure legend, the reader is referred to the web version of this article.)

purplish color of CME flame is due to the different reaction pathways of burning an oxygenated fuel, which was also studied by Chong et al. [6] in the case of sunflower biodiesel combustion.

The entire map of observed flame shapes is shown in Figs. 14 and 15. D is acting as a reference. Two conclusions are clear from Fig. 14. Distributed combustion is possible if T_{ca} is below 300 °C and p_g is at least 0.6 bar. MILD combustion requires high reactant inlet temperature to achieve distributed combustion, while MTC combustion requires relatively cool inlet streams to delay ignition and maintain distributed combustion. Therefore, excessively high temperature leads to quick ignition and a straight flame.

Flame shapes of all biodiesel test cases are summarized in Fig. 15.

The general criteria for distributed combustion are similar to that of D, i. e., high p_g and low T_{ca} are required. The low volatility of PME and WCO allows distributed combustion up to B25, then straight and transitory flames are observed with higher biodiesel concentrations. It was demonstrated in a preceding work that distributed combustion is possible with WCO if the equivalence ratio is increased [39]. However, excessive T_{ca} still narrows the accessible operating range for distributed combustion.

Low T_{ca} , which is 150 °C for the tested biodiesels, is insufficient for a stable flame for B75 and B100 fuels and B50 for PME. CME is an outlier in material properties and combustion characteristics, implying a correlation between thermophysical properties and flame shape. Distributed combustion of D was limited to $T_{ca} = 250$ °C, which holds for B25 biodiesels. However, more concentrated CME blends may feature distributed combustion up to $T_{ca} = 350$ °C with high atomization pressure. Another important observation is that the lower p_g limit is 0.45 bar for CME-B75 and B100. Consequently, it can be stated that stable distributed combustion shows a notable fuel sensitivity, regardless that D and biodiesels generally feature similar thermophysical properties compared to other fuels. As a guideline, MTC burners should be designed around specific fuels. At the same time, this technology can be considered fuel flexible in a reasonable parameter range, i.e., the trends were similar up to B25 independently of FAME composition due to the similar atomization and vaporization characteristics.

Figs. 16 and 17 present the measured NO emission converted to 15% flue gas oxygen level for easier comparison with new gas turbine power installation regulations. The 2015/2193 EU directive [33] allows 75 mg/Nm³ NO_x emission for new plants. Even though the currently used flue gas analyzer could measure the NO only, it is ~ 95% of the NO_x emission. The rest is NO₂, checked by a HORIBA MEXA 8120 flue gas analyzer, using reference measurement methods for all pollutants

		CME					PME					WCO				
		p_g [bar]					p_g [bar]					p_g [bar]				
T_{ca} [°C]		0.3	0.45	0.6	0.75	0.9	0.3	0.45	0.6	0.75	0.9	0.3	0.45	0.6	0.75	0.9
B25	350	s	s	s	s	s	s-d	s-d	s-d	s-d	s-d	s-d	s-d	s-d	s-d	s-d
	300	s	s	s	s	s	s	s-d	s-d	s-d	s-d	s-v	s-d	s-d	s-d	s-d
	250	s	s	s	s	s	s	s	s-d	s-d	d	s-v	s-d	s-d	s-d	s-d
	200	s	s	s	d	d	s	s-d	d	d	d	s	s	s	d	d
	150	s	s	s	s	d	s	s-d	s-d	d	d	s	s	d	d	d
B50	350	s	s	s	s	s	s	s	s-d	s-d	s-d	s-d	s-d	s-d	s-d	s-d
	300	s	s	s-d	d	d	s	s-d	s-d	s-d	s-d	s-v	s-d	s-d	s-d	s-d
	250	s	s-d	d	d	d	s	s-d	s	s	s	s-v	s-d	s-d	s-d	s-d
	200	s	s	s	d	d	s	s	s	s	s	s	s	s	s	s
	150	s	s	d	d	d						s	s	s	s	s
B75	350	s	s	s-d	d	d	s-d	s-d	s	s	s	s-d	s-d	s-d	s-d	s-d
	300	s	s-d	d	d	d	s	s	s	s-d	s-d	s-d	s-d	s-d	s-d	s-d
	250	s-d	d	d	d	d	s	s	s	s	s	s-d	s-d	s-d	s-d	s-d
	200	s	d	d	d	d	s	s	s	s	s-d	s	s-d	s-d	s-d	s-d
	150															
B100	350	s	s	s	s	s	s	s-d	s-d	s-d	s-d	s-v	s-d	s-d	s-d	s-d
	300	s	s-d	d	d	d	s	s-d	s-d	s-d	s-d	s-v	s-d	s-d	s-d	s-d
	250	s	d	d	d	d	s	s	s	s	s	s-v	s-d	s-d	s-d	s-d
	200	s	s-d	d	d	d	s	s	s	s	s-d	s	s-d	s-d	s-d	s-d
	150															

Fig. 15. Observed flame shapes at all biodiesel-diesel measurement points. Abbreviations referring to the flame shapes: s – straight (yellow), d – distributed (blue), v – V-shaped. Transitory operations (green: including distributed combustion and pink: including V-shaped flame), no stable combustion (hatched). CME data is from [32]. (For interpretation of the references to color in this figure legend, the reader is referred to the web version of this article.)

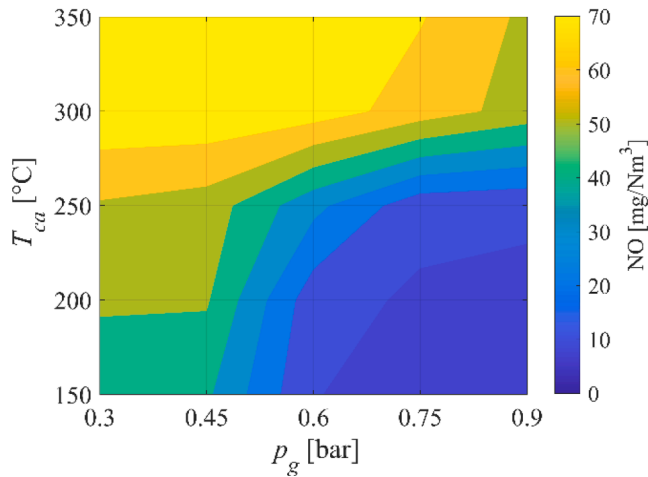


Fig. 16. NO emission of diesel combustion at 15% oxygen level. Data is from [32].

instead of electrochemical cells. This finding is in line with literature data [40]. The NO emission of some of the luminous yellow flames at low atomizing pressure and high combustion air temperature exceeded the 75 mg/Nm^3 limit; the highest NO concentration of biodiesels was 82 mg/Nm^3 , measured during WCO combustion. The highest NO emission of diesel combustion was 90 mg/Nm^3 . Please see all the measured values in Appendix C.

For the industry, the critical result is the NO emission reduction ratio between the different flame shapes. Note that the plots use linear interpolation; therefore, a mesh grid was added to indicate the measurement points. By comparing Figs. 14 and 16 for D, and Figs. 15 and 17 for biodiesels, the NO emission spectacularly correlates with flame shape. This is due to the disappearing hot local regions, which come with reduced NO_x emission. Combustion air preheating facilitates NO_x formation as the overall mixture temperature increases; therefore, the adiabatic flame temperature is higher, and exponentially increasing NO_x emission is expected [41]. If stable distributed combustion is reached, NO_x emission drops drastically. By maintaining distributed combustion, the NO_x emission can be kept below 14 mg/Nm^3 , which may also comply with the upcoming emission regulations. The highest NO emission of distributed combustion was measured for diesel, 13.8 mg/Nm^3 , while the maximum for biodiesel-diesel blends was 12.3 mg/Nm^3 by

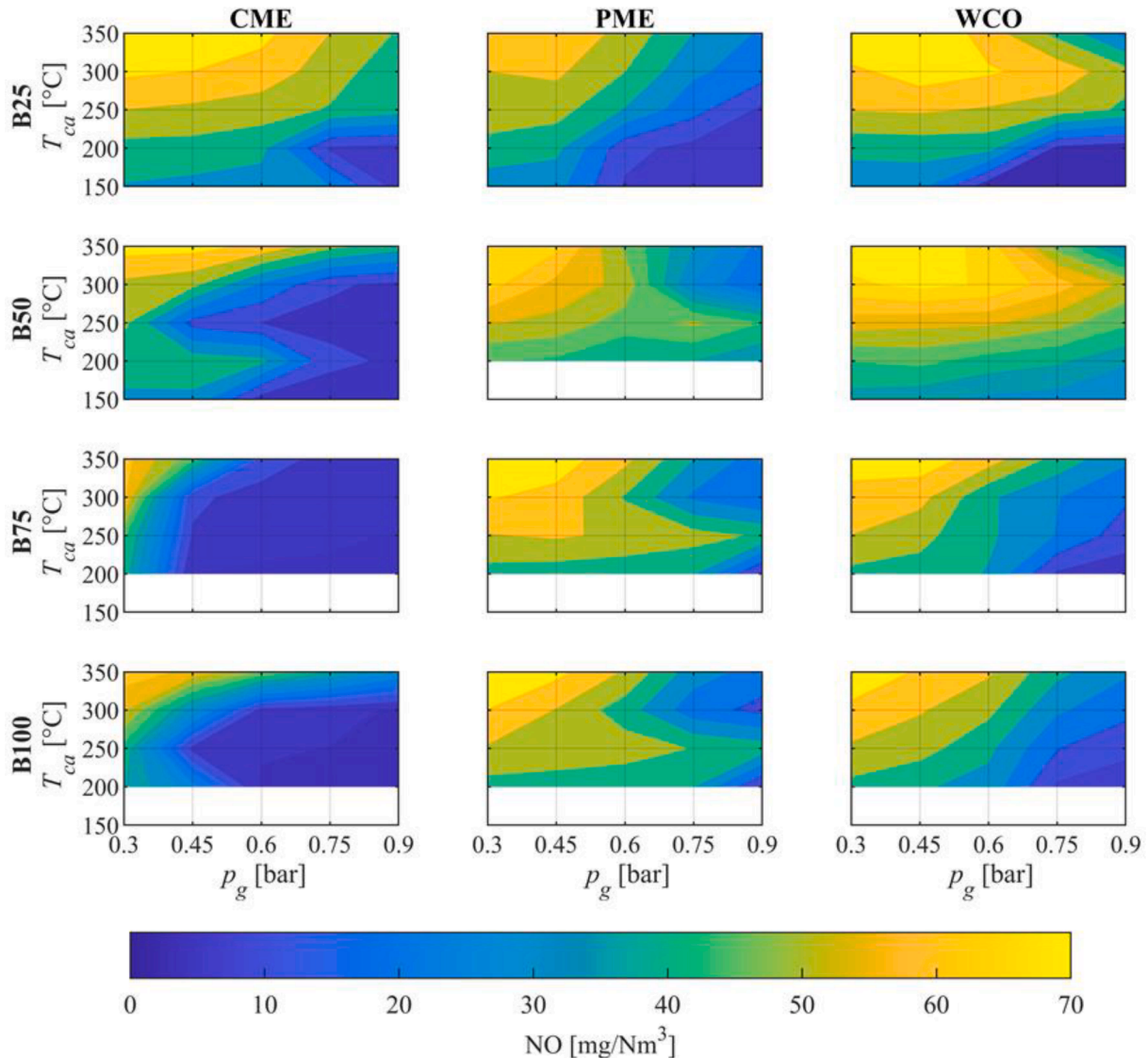


Fig. 17. NO emission of the combustion of biodiesel-diesel blends at 15% oxygen level.

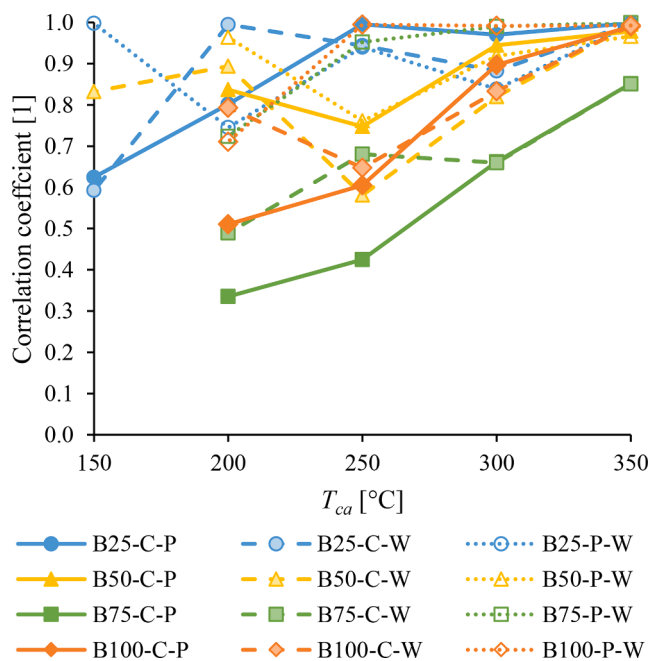


Fig. 18. Correlation coefficients of the comparisons of NO data of various fuel pairs at different T_{ca} values. C, P, and W are abbreviated CME, PME, and WCO here.

CME-B50. The average NO reduction from straight to distributed flames was 35.5 mg/Nm³ for D, 45.7 mg/Nm³ for CME blends, 42.6 mg/Nm³ for PME blends, and 27.1 mg/Nm³ for WCO blends, which means 78.2%, 88.1%, 82.9%, and 66.3% NO reduction, respectively. The average NO emission of distributed flames was < 10 mg/Nm³, the highest for D, 9.9 mg/Nm³, and the lowest for WCO, 4.1 mg/Nm³. The average NO of straight flames varied between 40.9 and 51.9 mg/Nm³. Note that the highest NO emission was not always in the case of stable straight flames, but mainly for the lowest p_g and highest T_{ca} , where transitory flames of straight and distributed shapes could be observed in some cases. Comparing the three biodiesels, CME exhibits the lowest NO emissions due to the lowest unsaturation level for CME, and the double bonds tend to lead to more acetylene formation, which is a precursor for NO_x, especially when in the presence of O₂. This result is consistent with the finding of Chiong et al. [42], as they showed that unsaturated biodiesels, such as coconut, emit lower NO_x than saturated biodiesels. Moreover, according to its molecular composition, CME has the highest oxygen content, with 14.5 m/m%, as shown in Table 3. The oxygen content of PME and WCO is 11.3 m/m% and 11.0 m/m%, meaning a higher lower heating value for these fuels, according to [43]. Therefore CME features the lowest adiabatic flame temperature.

By comparing all the biodiesel emission data to baseline diesel, biodiesels have lower emissions during distributed combustion. Still, CME and PME have higher peaks at straight flames, which results in a more spectacular NO_x drop between the two flame shapes. For all fuels and measurement setups, CO emission was below the measurement threshold, which means that combustion was practically complete.

Finally, a correlation analysis is performed on the NO emission data, considering all permutations. The calculations were all performed in Matlab, using the *corrcoef* function:

$$C(A, B) = \frac{1}{N-1} \sum_{i=1}^N \left(\frac{A_i - \mu_A}{\text{std}(A)} \right) \left(\frac{B_i - \mu_B}{\text{std}(B)} \right), \quad (5)$$

where C is the correlation coefficient, and A and B are random variables. μ is the mean, and the *std* operator stands for standard deviation. In the present case, the NO data of each fuel was evaluated at constant T_{ca} values. This choice supported that this variable greatly influenced

distributed combustion, leading to nearly a magnitude drop in emissions. Consequently, data sets with varying p_g were compared. The results are presented in Fig. 18.

The results show that all trends feature fluctuations; no smooth correlation exists. Since the material and evaporation properties of PME and WCO were the closest, the C of the data sets varies between 0.634 and 1, having a 0.904 mean and std of 0.118. Even though the correlation between CME and either PME or WCO peaked at 0.998 and 0.997, respectively, the minima were 0.335 and 0.489, caused by the greater tendency for distributed combustion at the same settings due to its lower volatility. The mean and std were 0.775, 0.207 for PME, and 0.802 and 0.153 for WCO, concluding that the trends of CME were closer to WCO.

4. Conclusions

This paper discusses the measured combustion-relevant thermo-physical properties of three biodiesels, CME, PME, and WCO, and their blends with commercial diesel fuel. These are density, viscosity, and surface tension critical for estimating atomization characteristics. Distillation curve measurement reveals fuel volatility in a high-temperature environment, while flash point describes fuel ignition properties. Then all the neat and blended fuels were analyzed in an MTC burner, offering distributed combustion without low-oxygen dilution. The following conclusions were derived:

1. The initial boiling point up to B25 blends is practically identical for all samples, exponentially increasing with biodiesel concentration. The rest of the properties also showed low variation up to B25, resulting in similar flame shapes independently of FAME composition, indicating B25 as the fuel flexibility upper limit for steady-operating combustion systems.
2. All thermophysical data of PME and WCO were similar, meaning interchangeability between these fuels. This finding was also supported by the correlation analysis based on NO emission data. The frying process showed no notable effect on the combustion characteristics.
3. A stable distributed combustion regime can be notably extended with proper fuel volatility, demonstrated by CME-B75. Distributed combustion and the accompanying favorable NO emission are accessible via increased atomizing pressure and low combustion air preheating.
4. The NO emission of distributed combustion could be kept below 14 mg/Nm³ at 15% flue gas oxygen content in all cases, which corresponds to, on average, an 80% NO reduction between straight and distributed flames. The lowest average emission was measured for WCO blends, 4.1 mg/Nm³, while the highest corresponds to D, with 13.8 mg/Nm³.

Funding

The research reported in this paper was supported by the National Research, Development and Innovation Fund of Hungary, project N^o.s OTKA-FK 124704, 137,758 and TKP2021 Grant N^o. BME-NVA-02, by the Ministry of Innovation and Technology of Hungary from the National Research, Development and Innovation Fund, N^o.s. ÚNKP-22-5-BME-304 and ÚNKP-22-3-II-BME-113, supported by the New National Excellence Program of the Ministry for Culture and Innovation from the source of the National Research, Development and Innovation Fund, and the János Bolyai Research Scholarship of the Hungarian Academy of Sciences.

Declaration of Competing Interest

The authors declare that they have no known competing financial interests or personal relationships that could have appeared to influence the work reported in this paper.

Data availability

We have already shared part of the experimental data in an online

repository which is referred in the manuscript and available for the readers and reviewers.

Appendix A. Fitted coefficients for initial boiling point, flash point, density, kinematic viscosity, and surface tension

Curve fitting was performed for the analyzed fuel properties to facilitate further calculations, leading to Eqs. (A.1)–(A.5):

$$T_{IBP} = b_1 \cdot e^{b_2 \cdot V} + b_3, \quad (\text{A.1})$$

$$T_{FP} = f_1 \cdot e^{f_2 \cdot V} + f_3, \quad (\text{A.2})$$

$$\rho_L = d_1 \cdot T + d_2 \quad (\text{A.3})$$

$$\nu_L / \nu_{L,40^\circ\text{C}} = k_1 \cdot (T/40^\circ\text{C})^{k_2} \quad (\text{A.4})$$

$$\sigma = s_1 \cdot T + s_2 \quad (\text{A.5})$$

where V is the biodiesel volume fraction in % and T is the temperature in $^\circ\text{C}$, and $\nu_{L,40^\circ\text{C}}$ is the kinematic viscosity in mm^2/s at 40°C . The corresponding coefficients are summarized in Tables (A.1)–(A.3).

Table A1

Parameters of Eqs. (A.1) and (A.2) for initial boiling point and flash point.

	CME	PME	WCO
b_1	3.820	2.909	7.786
b_2	0.02388	0.3670	0.02808
b_3	225.7	228.7	221.3
f_1	15.08	2.176	3.771
f_2	0.01347	0.03838	0.03303
f_3	70.40	83.20	81.06

Table A2

Parameters of Eqs. (A.3)–(A.5) for density, kinematic viscosity, and surface tension I.

	D	CME-B100	PME-B100	WCO-B100
d_1	−0.6920	−0.7477	−0.6906	−0.6942
d_2	834.5	885.5	884.4	891.9
k_1	0.9744	1.001	0.9825	0.9846
k_2	−0.8844	−0.8873	−0.9992	−1.018
s_1	−0.07629	−0.07808	−0.07037	−0.07808
s_2	28.50	30.39	31.82	32.58

Table A3

Parameters of Eqs. (A.3)–(A.5) for density, kinematic viscosity, and surface tension II.

	CME			PME			WCO		
	B25	B50	B75	B25	B50	B75	B25	B50	B75
d_1	−0.6925	−0.6905	−0.7264	−0.7182	−0.6800	−0.6566	−0.6939	−0.7023	−0.6936
d_2	846.6	857.0	873.0	848.9	858.5	870.7	848.3	863.2	877.8
k_1	0.9987	0.9605	0.9733	1.002	0.9896	0.9784	0.9973	0.9579	0.9768
k_2	−0.8389	−0.8578	−0.8967	−0.8701	−0.9225	−0.9746	−0.8224	−0.8904	−0.9405
s_1	−0.07482	−0.07376	−0.07389	−0.07379	−0.06935	−0.07301	−0.07617	−0.07038	−0.07071
s_2	28.81	29.39	29.50	29.03	29.18	30.88	29.50	28.99	30.47

Appendix B. Density, kinematic viscosity, and surface tension data

Table B.1 summarizes the temperature-dependent density, kinematic viscosity, and surface tension of the investigated fuel blends. SMD calculations were based on these measured values. Note that all the measured fuel properties discussed in this paper are available in [37] with the corresponding uncertainty values.

Table B1

Temperature-dependent density, kinematic viscosity, and surface tension data of the investigated fuel blends.

T [°C]		30	40	55	70	85	95
D	ρ_L [kg/m ³]	814.0	807.0	796.3	785.7	775.8	769.0
	ν_L [mm ² /s]	2.597	2.104	1.598	1.269	1.020	0.894
	σ [mN/m]	26.24	25.43	24.29	23.16	22.03	–
CME-B25	ρ_L [kg/m ³]	826.1	818.7	808.5	798.0	787.5	781.1
	ν_L [mm ² /s]	2.824	2.227	1.703	1.433	1.174	1.043
	σ [mN/m]	26.55	25.82	24.7	23.59	22.43	–
CME-B50	ρ_L [kg/m ³]	836.3	829.9	818.3	808.5	798.4	791.6
	ν_L [mm ² /s]	2.861	2.381	1.775	1.437	1.161	1.026
	σ [mN/m]	27.19	26.45	25.31	24.2	23.15	–
CME-B75	ρ_L [kg/m ³]	850.4	844.8	833.1	822.5	810.7	804.1
	ν_L [mm ² /s]	3.146	2.545	1.925	1.529	1.222	1.058
	σ [mN/m]	27.24	26.57	25.5	24.3	23.21	–
CME-B100	ρ_L [kg/m ³]	862.9	855.9	844.1	833.8	821.9	814.3
	ν_L [mm ² /s]	3.512	2.722	2.069	1.697	1.389	1.226
	σ [mN/m]	28.02	27.3	26.11	24.94	23.74	–
PME-B25	ρ_L [kg/m ³]	826.5	820.7	810.2	798.4	787.7	780.5
	ν_L [mm ² /s]	3.186	2.480	1.895	1.580	1.272	1.132
	σ [mN/m]	26.79	26.09	25.02	23.87	22.74	–
PME-B50	ρ_L [kg/m ³]	838.0	831.4	821.0	811.2	800.8	793.7
	ν_L [mm ² /s]	3.724	2.923	2.261	1.756	1.396	1.213
	σ [mN/m]	27.1	26.41	25.33	24.34	23.28	–
PME-B75	ρ_L [kg/m ³]	850.9	844.6	834.4	824.8	814.8	808.4
	ν_L [mm ² /s]	4.368	3.424	2.531	1.997	1.541	1.342
	σ [mN/m]	28.69	27.95	26.9	25.77	24.67	–
PME-B100	ρ_L [kg/m ³]	863.8	856.8	846.5	835.9	825.4	819.2
	ν_L [mm ² /s]	5.449	4.217	3.129	2.407	1.891	1.620
	σ [mN/m]	29.7	29.01	27.94	26.9	25.83	–
WCO-B25	ρ_L [kg/m ³]	827.0	821.0	810.3	799.5	789.3	782.3
	ν_L [mm ² /s]	3.174	2.519	1.937	1.609	1.349	1.207
	σ [mN/m]	27.17	26.46	25.33	24.23	22.96	–
WCO-B50	ρ_L [kg/m ³]	842.3	835.3	824.6	813.3	803.6	796.9
	ν_L [mm ² /s]	3.661	3.037	2.261	1.819	1.426	1.228
	σ [mN/m]	26.9	26.16	25.11	24.06	23.02	–
WCO-B75	ρ_L [kg/m ³]	857.0	850.3	838.9	829.9	818.7	811.8
	ν_L [mm ² /s]	4.442	3.532	2.653	2.120	1.614	1.402
	σ [mN/m]	28.35	27.65	26.57	25.51	24.47	–
WCO-B100	ρ_L [kg/m ³]	871.2	864.0	853.8	843.5	832.6	826.2
	ν_L [mm ² /s]	5.570	4.268	3.123	2.426	1.896	1.633
	σ [mN/m]	30.21	29.46	28.35	27.12	25.92	–

Appendix C. NO concentrations at 15% flue gas oxygen content

Figs. C.1 and C.2 show the measured NO emission at 15% flue gas oxygen content for diesel and biodiesel combustion. Values higher than the 75 mg/Nm³ limit according to the 2015/2193 EU directive [33] are highlighted in red.

D	p_g [bar]				
	T_{ca} [°C]	0.3	0.45	0.6	0.75
350	89.9	85.9	82.0	70.7	58.0
300	77.6	77.6	75.1	65.3	56.0
250	58.9	55.5	32.9	13.3	11.78
200	51.6	51.1	13.8	8.4	7.4
150	42.7	41.7	10.3	6.9	7.4

Fig. C1. NO emission (mg/Nm³) at all measurement points at 15% flue gas oxygen content of diesel combustion. Values exceeding the 75 mg/Nm³ limit according to the 2015/2193 EU directive [35] are red. Colors refer to the stable flame shapes: straight (yellow), distributed (blue), and transitory (green).

		CME					PME					WCO				
		p_g [bar]					p_g [bar]					p_g [bar]				
T_{ca} [°C]		0.3	0.45	0.6	0.75	0.9	0.3	0.45	0.6	0.75	0.9	0.3	0.45	0.6	0.75	0.9
B25	350	81.0	81.0	72.7	59.9	49.1	68.8	67.8	57.0	39.8	28.5	81.0	82.0	64.3	47.1	26.5
	300	71.7	69.7	65.8	55.0	42.7	59.9	61.9	50.1	31.9	24.1	67.3	75.1	71.2	65.8	53.5
	250	59.9	57.9	55.0	49.1	44.2	57.5	54.0	39.3	23.1	7.9	60.4	61.4	58.9	56.0	48.1
	200	46.7	46.2	42.7	8.3	6.4	45.7	42.7	12.8	6.9	6.4	42.1	44.2	43.7	7.4	3.9
	150	39.3	37.3	35.8	30.0	5.9	34.9	33.4	8.8	6.9	5.9	32.9	32.9	3.4	3.4	2.5
B50	350	74.2	73.7	67.8	53.0	44.7	69.2	66.3	49.1	35.4	23.1	73.7	75.1	67.3	48.1	32.4
	300	57.5	52.5	28.5	11.3	7.9	66.8	58.4	53.5	29.5	19.2	68.8	71.7	69.2	62.4	53.5
	250	52.5	15.7	9.8	7.4	6.4	55.5	53.5	47.6	51.1	45.2	57.5	56.5	56.0	52.1	46.2
	200	44.2	46.2	42.7	12.3	8.3	45.2	44.2	40.3	39.8	35.4	45.2	46.7	42.7	40.8	35.8
	150	38.3	37.8	4.9	4.4	4.4						37.8	36.3	33.9	32.9	29.0
B75	350	61.9	47.1	13.8	7.4	5.9	77.1	75.1	62.9	40.3	24.1	77.1	75.6	64.8	46.7	31.9
	300	60.9	11.3	7.4	5.4	5.4	70.7	66.8	49.1	28.0	20.1	64.3	63.3	41.7	30.4	21.6
	250	46.2	9.3	6.4	5.4	4.9	59.4	61.4	57.9	54.0	48.6	59.9	53.0	41.7	29.5	13.8
	200	42.7	4.9	4.4	4.4	4.4	46.2	44.7	43.2	40.8	6.4	47.1	46.2	39.3	8.3	5.4
	150															
B100	350	62.4	58.9	49.6	39.8	29.5	76.6	72.7	58.9	34.9	25.5	77.1	68.8	61.4	42.7	31.4
	300	56.0	32.9	7.9	6.4	4.4	69.7	59.4	44.7	24.1	16.7	67.3	60.9	52.5	31.4	23.1
	250	43.2	8.3	5.4	4.9	3.4	58.9	58.4	55.0	49.6	45.7	58.4	54.0	42.2	20.1	11.3
	200	40.3	27.0	4.4	3.4	3.4	46.2	43.7	42.7	40.3	7.9	47.1	41.3	36.3	8.3	6.9
	150															

Fig. C2. NO emission (mg/Nm^3) at all measurement points at 15% flue gas oxygen content of biodiesel-diesel combustion. Values exceeding the $75 \text{ mg}/\text{Nm}^3$ limit according to the 2015/2193 EU directive [35] are red. Colors refer to the stable flame shapes: straight (yellow), distributed (blue), transitory of straight-distributed (green), and transitory of straight-V-shaped (pink).

References

- [1] Buira D, Tovilla J, Farbes J, Jones R, Haley B, Gastelum D. A whole-economy Deep Decarbonization Pathway for Mexico. *Energy Strateg Rev* 2021;33:100578. <https://doi.org/10.1016/j.esr.2020.100578>.
- [2] Pan X, Wang H, Wang L, Chen W. Decarbonization of China's transportation sector: In light of national mitigation toward the Paris Agreement goals. *Energy* 2018;155: 853–64. <https://doi.org/10.1016/j.energy.2018.04.144>.
- [3] Iea. Installed power generation capacity by source in the Stated Policies Scenario, 2000–2040. Paris: IEA; 2019. accessed May 1, 2020.
- [4] Sepulveda NA, Jenkins JD, de Sisternes FJ, Lester RK. The Role of Firm Low-Carbon Electricity Resources in Deep Decarbonization of Power Generation. *Joule* 2018;2: 2403–20. <https://doi.org/10.1016/j.joule.2018.08.006>.
- [5] Intergovernmental Panel on Climate Change. Climate Change 2022: Mitigation of Climate Change 2022. <https://www.ipcc.ch/report/ar6/wg3/> (accessed May 1, 2022).
- [6] Environmental Protection Agency. Greenhouse Gas Emissions 2022. <https://www.epa.gov/ghgemissions/overview-greenhouse-gases> (accessed June 20, 2022).
- [7] Lefebvre AH, Ballal DR. Gas turbine combustion. third. Boca Raton: CRC Press; 2010. 10.1201/9781420086058.
- [8] Correa SM. A Review of NOx Formation Under Gas-Turbine Combustion Conditions. *Combust Sci Technol* 1993;87:329–62. <https://doi.org/10.1080/00102209208947221>.
- [9] Cavaliere A, de Joannon M. Mild Combustion. *Prog Energy Combust Sci* 2004;30: 329–66. <https://doi.org/10.1016/j.pecs.2004.02.003>.
- [10] Jithin EV, Raghuram GKS, Keshavamurthy TV, Velamati RK, Prathap C, Varghese RJ. A review on fundamental combustion characteristics of syngas mixtures and feasibility in combustion devices. *Renew Sustain Energy Rev* 2021; 146:111178. <https://doi.org/10.1016/j.rser.2021.111178>.
- [11] Xing F, Kumar A, Huang Y, Chan S, Ruan C, Gu S, et al. Flameless combustion with liquid fuel: A review focusing on fundamentals and gas turbine application. *Appl Energy* 2017;193:28–51. <https://doi.org/10.1016/j.apenergy.2017.02.010>.
- [12] Józsa V. Mixture temperature-controlled combustion: A revolutionary concept for ultra-low NOx emission. *Fuel* 2021;291:120200. <https://doi.org/10.1016/j.fuel.2021.120200>.
- [13] Reddy VM, Trivedi D, Sawant D, Kumar S. Investigations on emission characteristics of liquid fuels in a swirl combustor. *Combust Sci Technol* 2015;187: 469–88. <https://doi.org/10.1080/00102202.2014.956098>.
- [14] Gjorgievski VZ, Markovska N, Pukšec T, Duić N, Foley A. Supporting the 2030 agenda for sustainable development: Special issue dedicated to the conference on sustainable development of energy, water and environment systems 2019. *Renew Sustain Energy Rev* 2021;143:59–62. <https://doi.org/10.1016/j.rser.2021.110920>.
- [15] Chiong MC, Chong CT, Ng JH, Lam SS, Tran MV, Chong WWF, et al. Liquid biofuels production and emissions performance in gas turbines: A review. *Energy Convers Manag* 2018;173:640–58. <https://doi.org/10.1016/j.enconman.2018.07.082>.
- [16] Wei H, Liu W, Chen X, Yang Q, Li J, Chen H. Renewable bio-jet fuel production for aviation: A review. *Fuel* 2019;254. <https://doi.org/10.1016/j.fuel.2019.06.007>.
- [17] Elkelay M, Alm-Eldin Bastawisi H, Esmail KK, Radwan AM, Panchal H, Sadasivuni KK, et al. Experimental studies on the biodiesel production parameters optimization of sunflower and soybean oil mixture and DI engine combustion, performance, and emission analysis fueled with diesel/biodiesel blends. *Fuel* 2019; 255:115791. <https://doi.org/10.1016/j.fuel.2019.115791>.
- [18] Singh A, Sinha S, Choudhary AK, Panchal H, Elkelay M, Sadasivuni KK. Optimization of performance and emission characteristics of CI engine fueled with Jatropha biodiesel produced using a heterogeneous catalyst (CaO). *Fuel* 2020;280: 118611. <https://doi.org/10.1016/j.fuel.2020.118611>.
- [19] Chen H-G, Zhang Y-H-P. New bio-refineries and sustainable agriculture: Increased food, biofuels, and ecosystem security. *Renew Sustain Energy Rev* 2015;47: 117–32. <https://doi.org/10.1016/j.rser.2015.02.048>.
- [20] Alalwan HA, Alminshid AH, Aljaafari HAS. Promising evolution of biofuel generations. *Subject review Renew Energy Focus* 2019;28:127–39. <https://doi.org/10.1016/j.ref.2018.12.006>.
- [21] Elkelay M, Kabeel AE, El Shenawy EA, Panchal H, Elbanna A, Bastawisi HAE, et al. Experimental investigation on the influences of acetone organic compound additives into the diesel/biodiesel mixture in CI engine. *Sustain Energy Technol Assessments* 2020;37:100614. <https://doi.org/10.1016/j.seta.2019.100614>.
- [22] Committee on Industry Research and Energy. Report on the proposal for a directive of the European Parliament and of the Council on the promotion of the use of energy from renewable sources (recast (COM(2016)0767 – C8-0500/2016 – 2016/0382(COD))). 2017.
- [23] Abdullah B, Syed Muhammad SAF ad, Shokravi Z, Ismail S, Kassim KA, Mahmood AN, et al. Fourth generation biofuel: A review on risks and mitigation strategies. *Renew Sustain Energy Rev* 2019;107:37–50. <https://doi.org/10.1016/j.rser.2019.02.018>.
- [24] Our World in Data. Renewable Energy 2020. <https://ourworldindata.org/renewable-energy> (accessed July 11, 2022).
- [25] European Commission. Sustainable aviation fuels – ReFuelEU Aviation 2021. https://ec.europa.eu/info/law/better-regulation/have-your-say/initiatives/12303-Sustainable-aviation-fuels-ReFuelEU-Aviation_en (accessed October 13, 2021).
- [26] Goh BHH, Chong CT, Ge Y, Ong HC, Ng JH, Tian B, et al. Progress in utilisation of waste cooking oil for sustainable biodiesel and biogas production. *Energy Convers Manag* 2020;223. <https://doi.org/10.1016/j.enconman.2020.113296>.

- [27] Vogel T, Wensing M. Effects of fuel composition on spray ignition under engine relevant conditions. Proc. 8th Int. Conf. Model. Diagnostics Adv. Engine Syst. COMODIA 2012, 2012, p. 317–22.
- [28] Glassman I, Yetter R. *Combustion*. 4th ed. Burlington: Academic Press; 2008.
- [29] Cerinski D, Vujanović M, Petranović Z, Baleta J, Samec N, Hriberšek M. Numerical analysis of fuel injection configuration on nitrogen oxides formation in a jet engine combustion chamber. *Energy Convers Manag* 2020;220:112862. <https://doi.org/10.1016/j.enconman.2020.112862>.
- [30] Farobie O, Hartulistiyoso E. Palm Oil Biodiesel as a Renewable Energy Resource in Indonesia: Current Status and Challenges. *Bioenergy Res* 2022;15:93–111. <https://doi.org/10.1007/s12155-021-10344-7>.
- [31] Hoekman SK, Broch A, Robbins C, Cenicerros E, Natarajan M. Review of biodiesel composition, properties, and specifications. *Renew Sustain Energy Rev* 2012;16:143–69. <https://doi.org/10.1016/j.rser.2011.07.143>.
- [32] Józsa V, Hidegh G, Kun-Balog A, Ng J-H-H, Chong CT. Ultra-low emission combustion of diesel-coconut biodiesel fuels by a mixture temperature-controlled combustion mode. *Energy Convers Manag* 2020;214:112908. <https://doi.org/10.1016/j.enconman.2020.112908>.
- [33] European Parliament. Directive (EU) 2015/2193 of the European Parliament and of the Council of 25 November 2015 on the limitation of emissions of certain pollutants into the air from medium combustion plants. *Off J Eur Union* 2015;313.
- [34] Csemány D, DarAli O, Rizvi SAH, Józsa V. Comparison of volatility characteristics and temperature-dependent density, surface tension, and kinematic viscosity of n-butanol-diesel and ABE-diesel fuel blends. *Fuel* 2022;312. <https://doi.org/10.1016/j.fuel.2021.122909>.
- [35] Lefebvre AH, McDonnell VG. *Atomization and Sprays*. Second. Boca Raton, FL: CRC Press; 2017.
- [36] Urbán A, Malý M, Józsa V, Jedelský J. Effect of liquid preheating on high-velocity airblast atomization: From water to crude rapeseed oil. *Exp Therm Fluid Sci* 2019;102:137–51. <https://doi.org/10.1016/j.expthermflusci.2018.11.006>.
- [37] Csemány D, DarAli O, Rizvi SAH, Józsa V. Density, kinematic viscosity, surface tension, distillation curve, and flash point data of diesel-biodiesel blends. 2021. <https://doi.org/10.5281/zenodo.6367766>.
- [38] Bachler C, Schober S, Mittelbach M. Simulated distillation for biofuel analysis. *Energy Fuels* 2010;24:2086–90. <https://doi.org/10.1021/ef901295s>.
- [39] Józsa V, Hidegh GT, Csemány D, Kardos RA, Chong CT. Dynamics and emission of nearly flameless combustion of waste cooking oil biodiesel in an ultra-low emission non-MILD swirl burner. *Fuel* 2022;319:123743. <https://doi.org/10.1016/j.fuel.2022.123743>.
- [40] Zhang Q, Yao M, Zheng Z, Liu H, Xu J. Experimental study of n-butanol addition on performance and emissions with diesel low temperature combustion. *Energy* 2012;47:515–21. <https://doi.org/10.1016/j.energy.2012.09.020>.
- [41] Correa sm.. A Review of NO x Formation Under Gas-Turbine Combustion Conditions. *Combust Sci Technol* 1993;87:329–62. <https://doi.org/10.1080/00102209208947221>.
- [42] Chiong MC, Chong CT, Ng JH, Tran MV, Lam SS, Valera-Medina A, et al. Combustion and emission performances of coconut, palm and soybean methyl esters under reacting spray flame conditions. *J Energy Inst* 2019;92:1034–44. <https://doi.org/10.1016/j.joei.2018.07.003>.
- [43] Channiwala SA, Parikh pp.. A unified correlation for estimating HHV of solid, liquid and gaseous fuels. *Fuel* 2002;81:1051–63. [https://doi.org/10.1016/S0016-2361\(01\)00131-4](https://doi.org/10.1016/S0016-2361(01)00131-4).